Available online at www.sciencedirect.com
ScienceDirect
Journal of Bionic Engineering 12 (2015) 504–517

The Improved Characteristics of Bionic Gabor Representations by Combining with SIFT Key-points for Iris Recognition

Yuanning Liu[1,2], Fei He[1,2], Xiaodong Zhu[1,2], Zhen Liu[3], Ying Chen[1,2,4], Ye Han[1,2], Lijiao Yu[1,2]

1. *College of Computer Science and Technology*, *Jilin University*, *Changchun* 130012, *China*
2. *Key Laboratory of Symbolic Computation and Knowledge Engineering of Ministry of Education*, *Jilin University*, *Changchun* 130012, *China*
3. *Graduate School of Engineering*, *Nagasaki Institute of Applied Science*, *Japan*
4. *College of Software*, *Nanchang Hangkong University*, *Nanchang* 330063, *China*

Abstract

Gabor filters are generally regarded as the most bionic filters corresponding to the visual perception of human. Their filtered coefficients thus are widely utilized to represent the texture information of irises. However, these wavelet-based iris representations are inevitably being misaligned in iris matching stage. In this paper, we try to improve the characteristics of bionic Gabor representations of each iris via combining the local Gabor features and the key-point descriptors of Scale Invariant Feature Transformation (SIFT), which respectively simulate the process of visual object class recognition in frequency and spatial domains. A localized approach of Gabor features is used to avoid the blocking effect in the process of image division, meanwhile a SIFT key point selection strategy is provided to remove the noises and probable misaligned key points. For the combination of these iris features, we propose a support vector regression based fusion rule, which may fuse their matching scores to a scalar score to make classification decision. The experiments on three public and self-developed iris datasets validate the discriminative ability of our multiple bionic iris features, and also demonstrate that the fusion system outperforms some state-of-the-art methods.

Keywords: iris recognition, bionic Gabor features, scale invariant feature transformation, support vector regression, score level fusion

doi: 10.1016/S1672-6529(14)60141-4

1 Introduction

Iris recognition is one of the most stable and reliable technology among biometric technologies. The desirable properties of irises such as uniqueness, stability, and noninvasiveness make iris recognition particularly suitable for human identification. The first iris recognition system was proposed by Daugman in 1993 and is still the state of the art technique used today[1]. Subsequently, a large number of algorithms have been presented to develop new iris practical systems with less control[2–5]. However, the commercial iris recognition system still has several problems, such as intra-class variations (*e.g.*, iris texture affected by ageing), inter-class similarities (leads to false acceptance), and noise in data (*e.g.*, illumination effect to iris image pixels)[6].

In our previous work[7], we tried to consolidate the robustness of iris Gabor features in iris matching step, and build a hyper sausage-like manifold for simulating the topological connectivity and continuity among all samples from a same pattern class in high dimensional Gabor feature space. This method requires adequate iris samples from a pattern class to fit an optimal fitting manifold, and therefore, it is much more favorable for video-based iris recognition. However, when the enrolled irises are deficient, the bionic Gabor features are still vulnerable and need to be improved. Therefore, differing from our previous works, we focus on the feature extraction stage in this paper rather than the iris matching step. This is because more distinctive characteristics may help distinguish an object from others in our visual system, while the discriminative information will be introduced to iris recognition system only in the

Corresponding authors: Xiaodong Zhu
E-mail: zhuxd@jlu.edu.cn

feature extraction step. Feature extraction methods can be divided into two major categories roughly: transform based approaches and geometric approaches[8]. The transform based approaches need to project the normalized iris images, where the ring-shaped (polar coordinates) irises have been converted to Cartesian coordinates, to a certain transform domain for observing their texture frequency distributions. Several representative works in this category include Gabor approaches[1], wavelet transform analysis based approaches[3] and intensity variation analysis based approaches[4]. Most of above-mentioned methods may observe invisible characteristics in transform domain, and exclude most noises from the assigned feature space. Among these transform ways, Gabor features are the most popular iris representations in existed iris recognition system. The reason is that Gabor filters fit the 2D spatial response profile of each simple cell in the least-squared error sense and provide a useful and reasonably accurate description of most spatial aspects of visual receptive fields[9]. With excellent direction and scale sensitivity, they thus are generally regarded as the most bionic filters corresponding to the visual perception of human[8]. However, they have two drawbacks: the iris texture informative loss due to the misalignment in polar transformation and hard to achieve true rotation invariance[10]. While another form of iris features, the geometric approaches, may represent irises using distinctive geometric properties and address the problem of iris misalignment and rotation. These methods will define some geometric descriptors to detect meaningful geometric key points or structures in the iris images without normalization. Several representative works to this category include key point detection[8] and Scale Invariant Feature Transformation (SIFT) based description[10]. But it is not so reliable to directly cope with the iris images involving the noises and the intensity of illumination in spatial domain. Thereby, these geometric features in spatial domain require effective feature selection before iris matching stage.

The foregoing introductions suggest that seldom iris feature extraction is flawless, and can fully address the existed key problems in iris recognition, such as illumination variations, environmental conditions, and device variations. A promising option is to combine multiple bionic features to compensate for the weakness of Gabor representations in particular situations. Raja Sekar *et al*. presented a fusion method of statistical and co-occurrence features extracted from the curvelet and ridgelet transformed images[11]. Manhattan distance and multiclass classifier with logistic function were used to generate their final classification results[12]. Tan *et al*. took ordinal measures, color analysis, texture representation and semantic information as iris features, and utilized weighted sum rule to generate the fused score for classification[13]. Gong *et al*. selected three wavelengths-bands to represent an iris, and then integrated them using the agglomerative clustering based on two-dimensional principal component analysis[14]. The fusion of multiple features is regarded as a positive step towards the development of extremely ambitious types of iris recognition[15]. However, the primary issue in the fusion of multiple features is to deal with the heterogeneous manifestations among various features.

In this paper, four novelties are provided to handle the above mentioned challenges in the characteristics of iris bionic representations. First, we formulate two different types of Gabor features to simultaneously describe the iris texture information from the energy spectrum and frequency domain, which are also adopted in our previous works[7]. The Gabor response magnitude is the model of orientation for the selective neuron in the primary visual cortex[16], while the Gabor phase can capture the information from the zero-crossing of wavelet[17]. An advantage of our multiple feature extraction is lower computational complexity because both features can be calculated by only one set of Gabor filters. Second, a new localized way for extracting local Gabor energy and phase features is proposed. Local features can offer a closer analysis of the uniqueness of the iris texture. But they are generally included in several irregular distributions in the iris image blocks such as crypts, freckles, coronas, stripes, furrows, *etc*.[18]. Therefore, we divided the Gabor response magnitude and phase to generate local feature vectors, where iris texture can be further preserved. Compared with the traditional localized mode of iris image division, our localized method occurs after convolution and avoids the blocking effect in the process of image division. Third, we also use SIFT key points as the geometric characteristics of iris images to simulate the process of visual object cognition in spatial domain. But we present a new feature selection strategy to discard the redundant SIFT keypoints. We evaluate the SIFT keypoint candi-

dates by their neighborhood magnitudes, and remove the probable misaligned keypoints. The last originality of this paper is the combination of multiple Gabor features and SIFT keypoints for iris classification. In the fusion, we prefer a more flexible score level fusion as opposed to a feature level fusion, which can hardly address the heterogeneity among various features, and a decision level fusion, which involves less information[19]. A robust and effective score fusion method based on Support Vector Regression (SVR) is presented in this paper. This method may fuse the matching scores from multiple local Gabor features and SIFT keypoints alignment using a non-linear, high-dimensional regression function, which will better fit the non-correlations among the matching scores from multiple bionic features. To our best knowledge, this is the first paper to discuss the fusion of multiple bionic iris features from both frequency and spatial domain.

The architecture of the proposed iris recognition system is shown in Fig. 1. As the standard procedures of iris recognition system, our system also includes iris image preprocessing, feature extraction and matching steps. Firstly, all iris images are preprocessed into a Region Of Interest (ROI) image before Gabor feature extraction to provide more precise iris templates[20]. Meanwhile, unlike our previous works, the segmented iris images are passed to SIFT keypoint extraction without normalization, according to its basic principle. During the feature extraction stage, as the core content of this paper, the local Gabor energy and phase representations are still produced by the same Gabor filters. At the same time, the innovative SIFT keypoints are detected and selected by their neighboring magnitudes. Next, all matching scores from two kinds of local Gabor features and SIFT keypoint alignment are sent into a trained SVR model, and are mapped to a single scalar score to make the final decision.

The remainder of this paper is organized as follows: Section **2** introduces the generation process of two types of local Gabor features and their matching scores. Section **3** illustrates our proposed discriminative SIFT keypoint extraction and selection. Section **4** describes the SVR based fusion scheme for multiple bionic iris features. The experimental results are discussed in Section **5**. Section **6** summaries this paper.

2 The iris local Gabor features

2.1 Gabor function

In the spatial domain, a general function of the two-dimensional Gabor kernel is defined as[21]

$$G_{\mu,\nu}(z)=\frac{\|k_{\mu,\nu}\|^2}{\sigma^2}e^{-\frac{\|k_{\mu,\nu}\|^2\|z\|^2}{2\sigma^2}}\left[e^{ik_{\mu,\nu}z}-e^{-\frac{\sigma^2}{2}}\right]. \quad (1)$$

From Eq. (1), we can see that the Gabor function is a product of a Gaussian envelope and a complex plane wave, where μ and ν determine the objective orientation and scale. The center of the receptive field is $z = (x, y)$. $\|\bullet\|$ denotes the norm operator. The standard derivation of the Gaussian envelope is σ, which determines the ratio of the Gaussian width to the wavelength. We adopt the DC-free Gabor kernel here that offers an invariance property to the ambient illumination change in the iris image acquisition[22]. The wave vector is defined as:

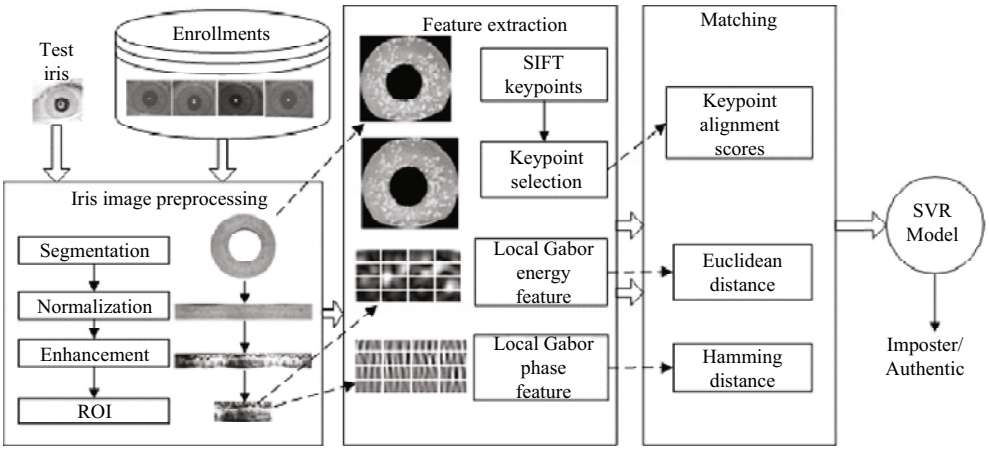

Fig. 1 The overview of the proposed iris recognition system.

$$k_{\mu,\nu} = k_\nu e^{i\varphi_\mu}, \tag{2}$$

$$e^{ik_{\mu,\nu}z} = \cos k_{\mu,\nu}z + i\sin k_{\mu,\nu}z, \tag{3}$$

where k_ν and ϕ_μ are the frequency and orientation of the targeted texture.

2.2 Multi-channel Gabor filters

A set of multi-channel Gabor filters should be used to provide the basis for distinguishing irises[23]. Due to the non-uniform frequency distribution of the iris texture and to obtain isotropy in the orientations, we choose transfer functions that have size variations and lattice discretization[24]. The selection of frequency k_ν in Eq. (3) can be computed as

$$k_\nu = K_{\max} / f^\nu, \quad \nu = 0,1,\ldots,M-1, \tag{4}$$

where $K_{\max}$ is the maximum frequency that defines the covered frequency band, M is the number of all extracted scales and f is the frequency scaling factor. An important wavelet property that provides the orthogonal basis to Gabor functions is inherited by following Eq. (4)[23]. The standard derivation σ can be achieved by $\sigma = K_{\max}/2(2^M - 1)$. The selection of targeted orientation ϕ_μ is calculated as

$$\varphi_\mu = \mu\pi/N, \quad \mu = 1,2,\ldots,N, \tag{5}$$

where N is the number of targeted orientations in Gabor transformation.

2.3 Two types of localized Gabor features and their matching scores

In this paper, we extract two different types of local Gabor features based on the Gabor filtered responses and their division. Using Gabor filtered response division for generating local Gabor features instead of image division can eliminate the blocking effect in the process of convolution. The blocking effect of image division will lead some staircase noises into Gabor transformation[25]. Even though several iris characteristics exist in a localized block, they will be degraded such that the block boundary looks like the edge. Further, the accuracy and reliability of Gabor features will be badly hurt. Therefore, we generate local Gabor features by dividing each Gabor response magnitude into $r\times c$ size blocks. The statistical means of all blocks constitute a local energy Gabor feature because the Gabor response magnitude is related to the local energy spectrum. Their matching score may be calculated using the Euclidean Distance (ED). To eliminate the effects of dimension, the L2 norm of each iris feature may be designated in the ED computation.

The second type of localized Gabor features called the local Gabor phase features is generated by dividing each Gabor response phase into $r\times c$ size blocks. Next, each block is encoded in accordance with signum operator[1]. Hamming Distance (HD) is used to compute across a population of unrelated phase codes bit-by-bit.

3 SIFT keypoint extraction

3.1 SIFT keypoint descriptor

SIFT method is capable of extracting and matching points which are stable and characteristic between two irises. It uses both image intensity and gradient information to characterize the neighborhood property of a given landmark. The first step is to construct a Gaussian scale space $L(x, y, \sigma)$. Thus the input image $I(x, y)$ is successively smoothed with a Gaussian function $G(x, y, \sigma)$ via Eq. (6).

$$L(x,y,\sigma) = G(x,y,\sigma) * I(x,y), \tag{6}$$

where

$$G(x,y,\sigma) = \frac{1}{2\pi\sigma^2} e^{-(x^2+y^2)/2\sigma^2},$$

and * is the convolution operation.

Next the Difference-of-Gaussian (DOG) images $D(x, y, \sigma)$ can be computed from the two nearby scales by a constant multiplicative factor k via Eq. (7).

$$D(x,y,\sigma) = L(x,y,k\sigma) - L(x,y,\sigma). \tag{7}$$

In order to detect the local minima and maxima of DOG images $D(x, y, \sigma)$, each pixel is compared to its eight neighbors in the current image and nine neighbors in the scale above and below, only the point which has the largest or smallest value among all of these neighbors will be selected[26] as keypoints. After determined the keypoints candidates, a main orientation is assigned to each keypoint based on local image gradients. For each image sample $L(x, y)$, the gradient magnitude $m(x, y)$ and orientation $\theta(x, y)$ are computed by Eq. (8) and Eq. (9), respectively.

$$m(x,y)=\sqrt{(L(x+1,y)-L(x-1,y))^2+(L(x,y+1)-L(x,y-1))^2}, \tag{8}$$

$$\theta(x,y)=\tan^{-1}\left(\frac{L(x,y+1)-L(x,y-1)}{L(x+1,y)-L(x-1,y)}\right). \tag{9}$$

Therefore, the keypoint descriptor can be characterized by the gradient magnitude and orientation around the keypoint location. Fig. 2 shows the process of keypoint descriptor formed.

As shown in Fig. 2a, the corresponding gradient magnitude and orientation of the pixels around Key-points are computed firstly. Then these pixels are accumulated into the orientation histograms summarizing the contents over 4×4 sub-regions. Each of them is represented by the length of each arrow corresponding to the sum of the gradient magnitudes, as shown in Fig. 2b.

Lowe pointed out the 4×4 array of histograms with 8 orientation bins for each keypoint may achieve the best results[26]. Hence, in our work we adopt 4×4×8=128 element feature vectors to represent a keypoint.

3.2 Discriminative feature selection and matching

From the above discussions, the SIFT key-points may contain redundant features. We present the way of Neighborhood Element Probability Distribution Function (NEPDF) to actualize the selection of keypoints.

Considering M SIFT key-points in an iris image, a matrix $\boldsymbol{S}$ with M rows and 128 columns can be formed for representing this iris. Let $S_{\alpha,\beta}$ denote the element in the αth row and the βth in the matrix $\boldsymbol{S}$. A vector $\boldsymbol{\mu}^{\alpha}$ can be obtained from the αth of $\boldsymbol{S}$ as Eq. (10).

$$\begin{aligned}\mu^{\alpha}&=\left[\upsilon_{\alpha,1},\upsilon_{\alpha,2},\cdots,\upsilon_{\alpha,15},\upsilon_{\alpha,16}\right]\\&=\left[\sum_{i=1}^{8}S_{\alpha,i},\sum_{i=9}^{16}S_{\alpha,i},\cdots,\sum_{i=113}^{120}S_{\alpha,i},\sum_{i=121}^{128}S_{\alpha,i}\right].\end{aligned} \tag{10}$$

Further the sum of neighborhood sub-region v_j can be computed via Eq. (11)

$$v_j=\sum_{i=1}^{M}\upsilon_{i,j},\quad j=1,\cdots,16. \tag{11}$$

Therefore, the NEPDF $P(v_j)$ can be calculated through Eq. (12).

$$P(v_j)=\frac{\sum_{i=1}^{M}\upsilon_{i,j}}{\sum_{i=1}^{M}\sum_{j=1}^{16}\upsilon_{i,j}}=\frac{\sum_{i=1}^{M}\sum_{m=8\times(j-1)}^{8\times j}S_{i,m}}{\sum_{i=1}^{M}\sum_{k=1}^{128}S_{i,k}},\ j=1,\cdots,16. \tag{12}$$

The NEPDF $P(v_j)$ is denoted as a vector $\boldsymbol{V}$, and $\boldsymbol{V}$=[v_1, v_2, …, v_{16}]. The elements $\boldsymbol{V}^{s}$ with minor value will be finitely deleted in our system.

Two images $\boldsymbol{I_1}$ and $\boldsymbol{I_2}$ are aligned by comparing each keypoint based on their associated descriptors[27]. For any point p_{11} from image $\boldsymbol{I_1}$, let its two closest neighbor key-points in image $\boldsymbol{I_2}$ denote p_{21} and p_{22}. We calculate the Euclidean distances d_1 and d_2, which respectively measure between p_{11} and p_{21} and between p_{11} and p_{22}, to determine the key-points p_{11} and p_{21} as matching pairs by the ratio d_1/d_2. If it is smaller than a predefined threshold value 0.85, the two points p_{11} and

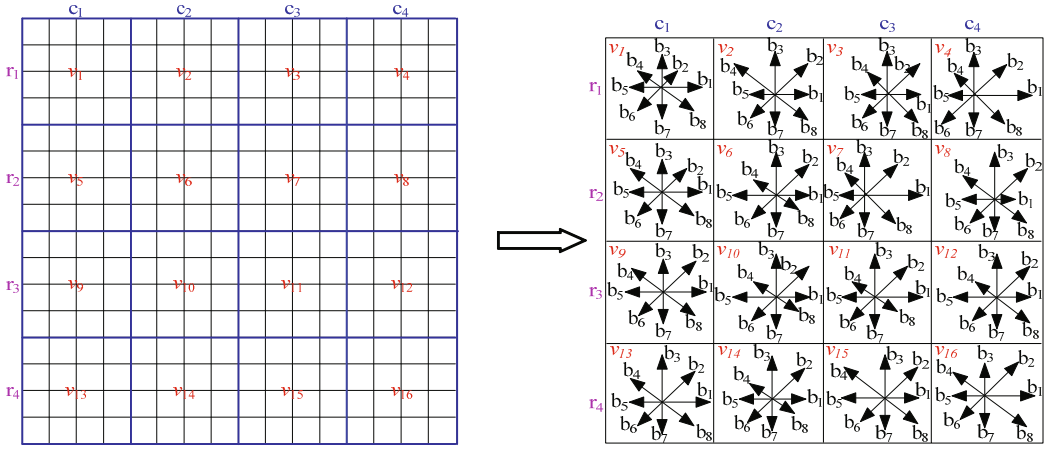

(a) Image gradients (b) Keypoint descriptor

Fig. 2 The process of keypoint detection.

p_{21} is be considered as a matching pair. The matching score between two images based on the proportion of the matched keypoints.

4 The fusion scheme based on SVR

In our system, after two types of local Gabor features and SIFT keypoints extraction, the combination of their discriminative ability should be considered. The matching score is a real value measuring the similarity between the input and template biometric feature vectors. In score level fusion, all real value scores from multiple bionic features will be combined into a real value to arrive at a final recognition decision. In its implementation, the linear weighted strategy was frequently used in some literatures[28]. However, in our work, due to the uncorrelated matching scores among Gabor and SIFT features, a non-linear fusion rule based on Support Vector Regression (SVR) is adopted. The idea of SVR is based on the computation of a regression function in a high-dimensional feature space where the input data are mapped via a nonlinear function[29]. The regression function $f(x)$ in SVR can be denoted as

$$f(x)=\sum_{i=1}^{k}(\beta_i^*-\beta_i)K(x,x_i)+b,\quad i=1,2,\cdots,k, \qquad (13)$$

where k is the number of training data. The Lagrangian multipliers β_i^*, β_i are found by solving a quadratic programming problem[30], and b is the bias. A kernel function $K(u, v)$ performs the non-linear mapping. Any symmetric function that satisfies Mercer's condition can be chosen as $K(u, v)$. The usual kernels include dot, polynomial, Radial Basis Function (RBF) and neuron kernels[31].

We take advantage of the SVR to fit a function $f(x)$, which may map multiple matching scores to a fused score to make the final decision of arbitrary one-to-one identity. The ED and HD of the local Gabor energy and phase features, together with the matching score of selected SIFT keypoints in a comparison are formed as an input vector. Because the matching scores have been normalized to [0, 1] real-value range, and this intrinsic characteristic just might naturally avoid the question of heterogeneous input of fusion. All input data with labels from arbitrary one-to-one comparisons of enrolled irises are used to train a SVR model. The authentic comparisons is labeled 0 as the observed value, while the imposter comparisons is labeled 1. In the forecast mode of trained SVR, an input score vector may be mapped to a real value as its fused score. This value can be considered to integrate Gabor and SIFT features to measure the similarity between two irises. A lower value (close to the authentic label) obtained by the output of SVR demonstrates that the test iris and the involved enrolled iris are in the same pattern class. In light of this principle, only a reasonable threshold should be chosen to complete the classification decision.

5 Experimental results

5.1 Datasets

For the purpose of sufficiently investigating iris recognition performance under changing illuminations, acquisition deflection, ageing and other circumstances, we established a large-scale JLUBR-IRIS dataset using our self-developed online iris image capture system[32]. The images in the JLUBR-IRIS dataset were gathered under various illumination levels from indoors. A class of samples from different acquisition times and different illumination levels is shown in Fig. 3.

In this paper, three datasets, including the JLUBR-IRIS, CASIA-I and CASIA-V4-Interval datasets, are used to examine the effectiveness of the proposed algorithm. Due to the weaker contrast of texture in the Asian iris as opposed to the European iris, all experimental subjects from the three chosen datasets are Chinese people to control comparability[33,34]. Table 1 shows the experimental settings for the three datasets.

Every iris image in Table 2 is manually selected from accurate iris region segmentation by the Canny operator and the Hough transformation to prevent interference caused by iris misalignment[35]. To evaluate the performance of our proposed local Gabor features

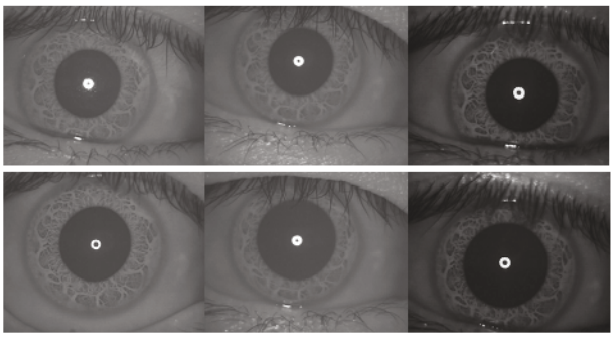

Fig. 3 Several iris images from a class in the JLUBR-IRIS dataset.

Table 1 The employed dataset descriptions

No	Dataset	Device	Resolution (pixels × pixels)	Attributions	User	Images	Gallery	Probe
1	CASIA-I	close-up camera	320 × 280	Graduate students	108	7	4	3
2	CASIA-V4-Interval	OKI IRISPASS-h	640 × 480	Graduate students	249	7–10	5	2–5
3	JLUBR-IRIS	OV7620	640 × 320	Graduate students and staffs	273	15	10	5

Table 2 The performance of proposed single bionic iris features and their fusion on three datasets

Dataset	Gabor energy features			Gabor phase features			Selected SIFT keypoints			Fusion		
	DI	*CRR*/%	*EER*/%	*DI*	*CRR*/%	*EER*/%	*DI*	*CRR*/%	*EER*/%	*DI*	*CRR*/%	*EER*/%
CASIA-I	3.59	97.83	2.85	3.82	98.98	1.87	3.63	98.10	3.01	4.54	99.98	0.19
CASIA-V4-Interval	3.37	95.16	3.93	3.86	98.78	1.04	3.50	96.62	3.61	4.38	99.51	0.54
JLUBR-IRIS	3.15	93.01	4.67	3.34	97.03	3.16	3.25	95.88	4.59	4.06	98.30	1.65

and fusion scheme, indicators Discriminative Index (*DI*), False Accept Rate (*FAR*), False Reject Rate (*FRR*) and Equal Error Rate (*EER*) are used. They can observe in graphing by DDH and Receiver Operating Characteristic (ROC) curves, which are plotting the *FAR* versus *FRR* with different values of matching threshold. These comparative indicators as the academic standard benchmark for iris recognition are applied to control the comparability of the experimental results.

5.2 Experimental results

In this section, we report the comparison between the different localized feature extraction methods for the three adopted iris datasets first. We use the empirical Gabor filters ($K_{max} = 64$, $f = 2$, $M = 6$, $N = 4$) introduced in Ref. [36] to extract the Gabor features. In this test, we divided ROI images to generate features that represent the existing localized method[37]. Various grid search-based block sizes are used to analyze two localized ways. Fig. 4 to Fig. 9 shows the relationships between *DI*s and block sizes in two localized means.

It can be concluded from Fig. 4 to Fig. 9 that the smallest block size is not the most suitable one for localized features. If the block size is focused excessively on the minute texture, the local features can not enhance the iris texture information but include redundant noises. Therefore, the block size of localization has to be adjusted for different batch samples. Furthermore, for the Gabor energy and phase features, our proposed localized way can obtain more powerful local features and conserve more texture in the process of image division and convolution. In all of the following experiments, the localized block size that obtains the best discriminative ability is adopted.

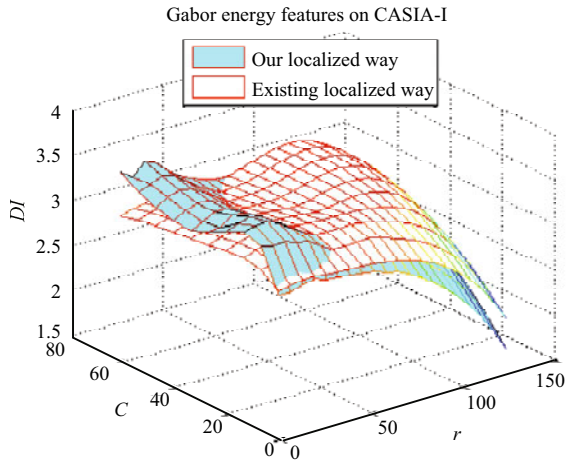

Fig. 4 The relationship between the *DI*s of the Gabor energy features and the block sizes in different localized ways on the CASIA-I dataset.

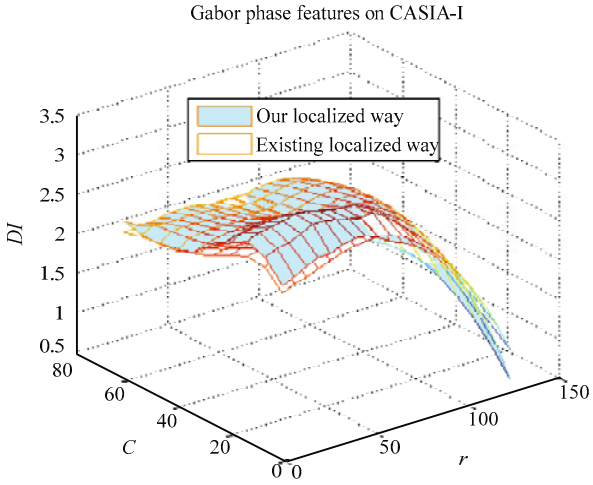

Fig. 5 The relationship between the *DI*s of the Gabor phase features and the block sizes in different localized ways on the CASIA-I dataset.

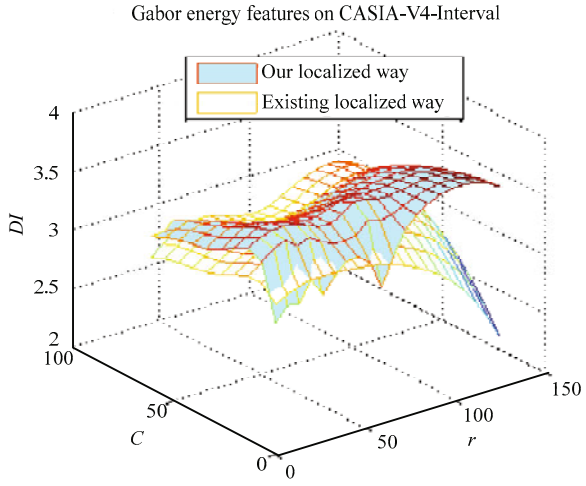

Fig. 6 The relationship between the *DI*s of the Gabor energy features and the block sizes in different localized ways on the CASIA-V4-Interval dataset.

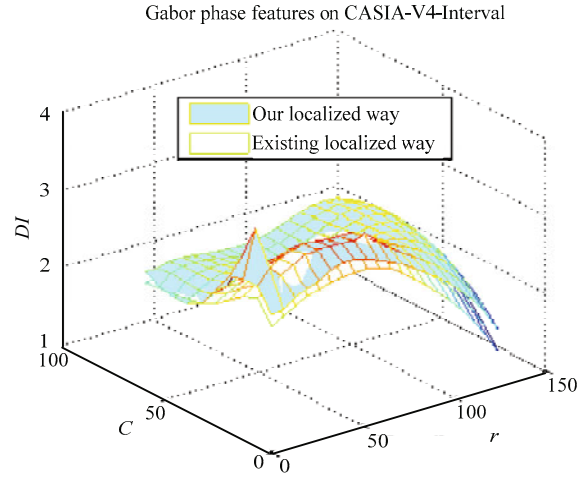

Fig. 7 The relationship between the *DI*s of the Gabor phase features and the block sizes in different localized ways on the CASIA-V4-Interval dataset.

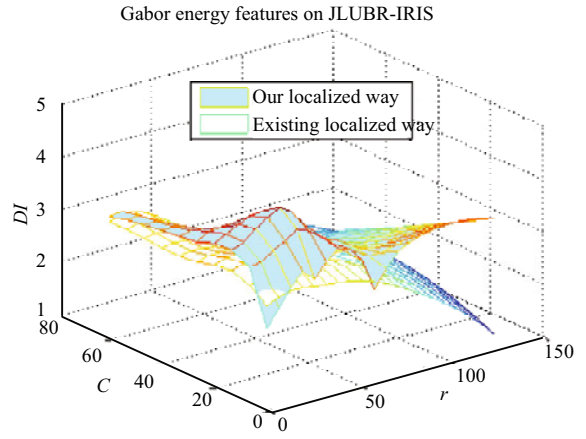

Fig. 8 The relationship between the *DI*s of the Gabor energy features and the block sizes in different localized ways on the JLUBR-IRIS dataset.

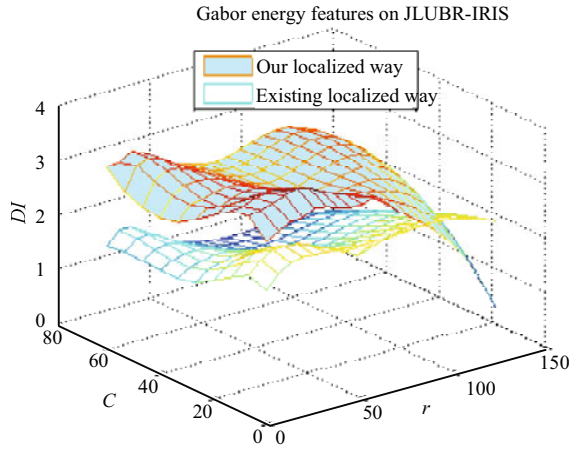

Fig. 9 The relationship between the *DI*s of the Gabor phase features and the block sizes in different localized ways on the JLUBR-IRIS dataset.

The second set of experiments is to select the optimal SIFT keypoints based on magnitude. We conduct the SIFT keypoint selection on three datasets, and count up the deleted candidate keypoints. The diagrams of percentage of deleted keypoints are shown in Fig. 10. As this figure shown, the average percentages of deleted keypoints are 2.43%, 2.89%, and 5.68% on the CASIA-I, CASIA-V4-Interval and JLUBR-IRIS datasets, respectively. They demonstrate that more noises and redundant interference exist in the JLUBR-IRIS dataset than the CASIA-I and CASIA-V4-Interval datasets.

In order to validate the selected SIFT keypoints, we implement the iris recognition using the gallery and probe sets on three datasets. The comparative ROC curves of SIFT keypoints and selected SIFT keypoints are shown in Fig. 11. From the ROC curves, the discriminative ability of the selected SIFT keypoints shows greater performance than traditional SIFT keypoints. This explains the fact that our SIFT keypoints selection may remove the meaningless and ambiguous keypoints from traditional SIFT, and consolidate the extracted geometric features. Put the ROC curves all together and the greatest improvement of performance among three datasets can be found on the JLUBR-IRIS dataset. That is because of more conditions and noises involved in its acquisition, which leads to embed unuseful but sensitive geometric properties in traditional SIFT keypoint detection. It is also the reason why the highest average percentage of deleted keypoints in our keypoint selection emerged in the JLUBR-IRIS dataset.

Subsequently, we try to combine the multiple local

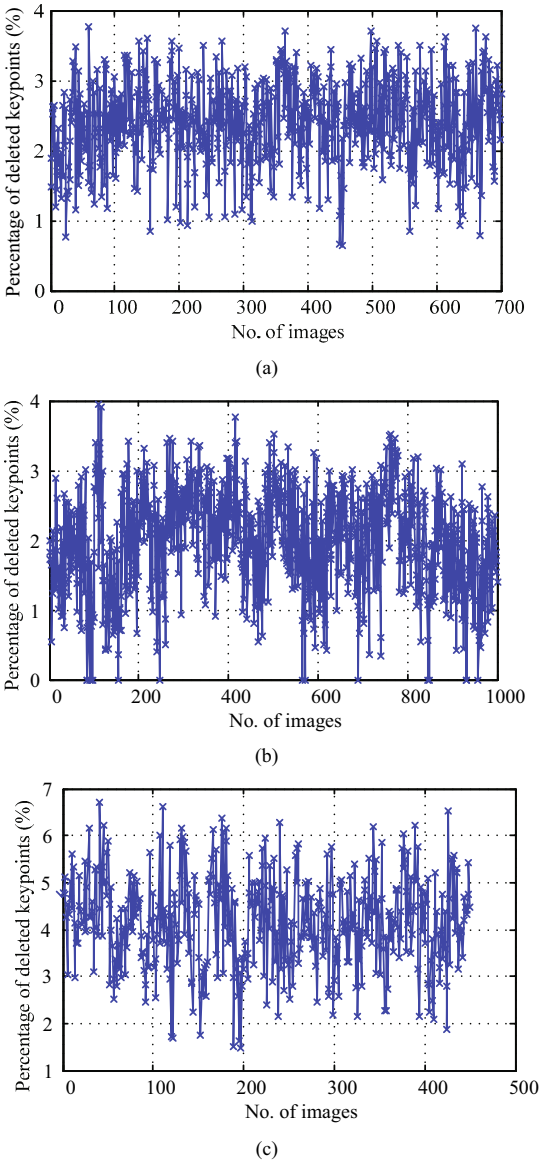

Fig. 10 The percentage of deleted keypoints on the (a) CASIA-I (b) CASIA-V4-Interval, and (c) JLUBR-IRIS datasets.

Gabor features and optimal SIFT keypoints for further improvement. The two local Gabor features and the SIFT keypoints after magnitude selection strategy are extracted to represent arbitrary iris sample for simulating the process of visual object class recognition in both frequency and spatial domains. Then our fusion scheme is launched to activate the integrated discriminative ability of multiple bionic iris features. Due to our fusion strategy, the matching scores of multiple bionic iris features from arbitrary one-to-one identity on the gallery set are combined for SVR modeling. These matching scores with their corresponding authentic or imposter labels are also sent to train the SVR model. In our fusion experiments, the commonly used RBF kernels are tried to train the best performed SVR model. After the SVR modeling, the probe sets of all users are provided to validate our proposed fusion scheme. In our experiments, the regression mode of LibSVM[38] is applied, where we can establish the four common kernels and check a grid of β_i^*, β_i parameters by the simple tool LibSVM provided. The RBF kernel reflected the non-linear correlation among multiple bionic iris features is employed here. The DDHs of fused scores based on the corresponding trained SVR model on three datasets are shown in Fig. 12. From the figures, the fused values from the authentic/imposter comparisons are much closer to the authentic label (0)/imposter label (1). Therefore, we can select a reasonable threshold to make the final decision.

We list the performance of above described each modal iris features and their fusion for comparisons in Table 2. We can read that the best performance is achieved by the fused scores. The predominant iris recognition performance, in terms of *DI*, *CRR* and *EER*, come from the fusion experiments on three datasets, which exhibits that our proposed SVR fusion strategy may bring the distinctive ability of all the bionic iris features into full play. In addition, the greatest improvement our fusion algorithm made among three datasets is generated on the JLUBR-IRIS dataset. This is due to its larger scale samples in gallery set and more training data involving in SVR modeling stage, which may achieve better distinctive regression function.

We also draw the comparative ROC curves of our proposed Gabor and SIFT bionic features and their fusion on three datasets as Fig. 13. In there, our fusion approaches obtain the lowest ROC curves and are superior to those of any Gabor and SIFT iris feature on three datasets. From above experiments, besides achieving improved local Gabor features and selected SIFT keypoint descriptors, our proposed system may combine their distinctive ability for performing more robust and reliable iris recognition.

In order to further exhibit the efficiency of our proposed approaches, we carry out the comparisons of our proposed method with some state-of-the-art methods in terms of *CRR* and *EER* on the CASIA-V4-Interval dataset. The comparative *CRR* and *EER* are listed in Table 3, which further demonstrate encouraging

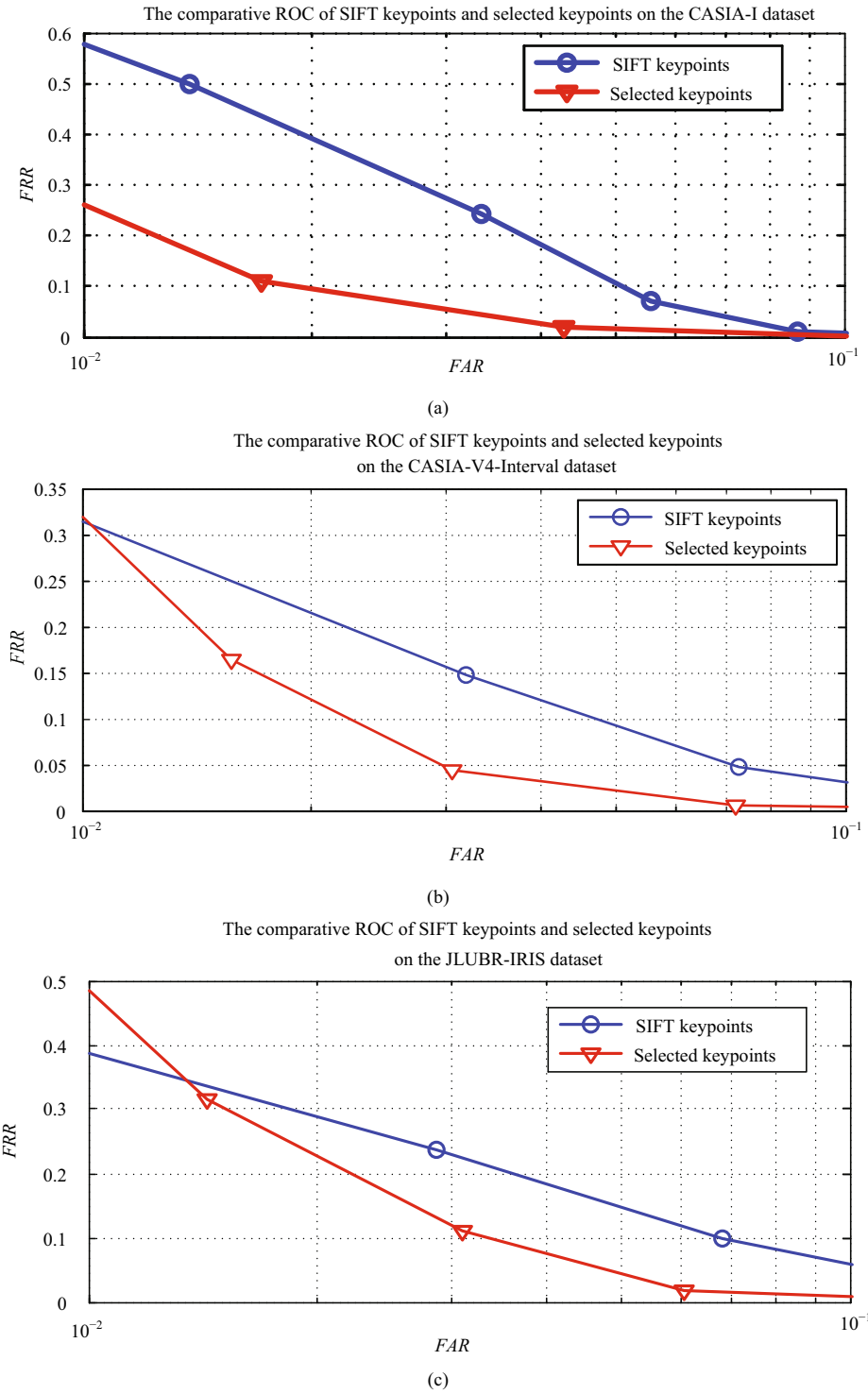

Fig. 11 The comparative ROC curves of SIFT keypoints and selected keypoints on the (a) CASIA-I, (b) CASIA-V4-Interval and (c) JLUBR-IRIS datasets.

Table 2 The performance of proposed single bionic iris features and their fusion on three datasets

Dataset	Gabor energy features			Gabor phase features			Selected SIFT keypoints			Fusion		
	DI	*CRR*/%	*EER*/%	*DI*	*CRR*/%	*EER*/%	*DI*	*CRR*/%	*EER*/%	*DI*	*CRR*/%	*EER*/%
CASIA-I	3.59	97.83	2.85	3.82	98.98	1.87	3.63	98.10	3.01	4.54	99.98	0.19
CASIA-V4-Interval	3.37	95.16	3.93	3.86	98.78	1.04	3.50	96.62	3.61	4.38	99.51	0.54
JLUBR-IRIS	3.15	93.01	4.67	3.34	97.03	3.16	3.25	95.88	4.59	4.06	98.30	1.65

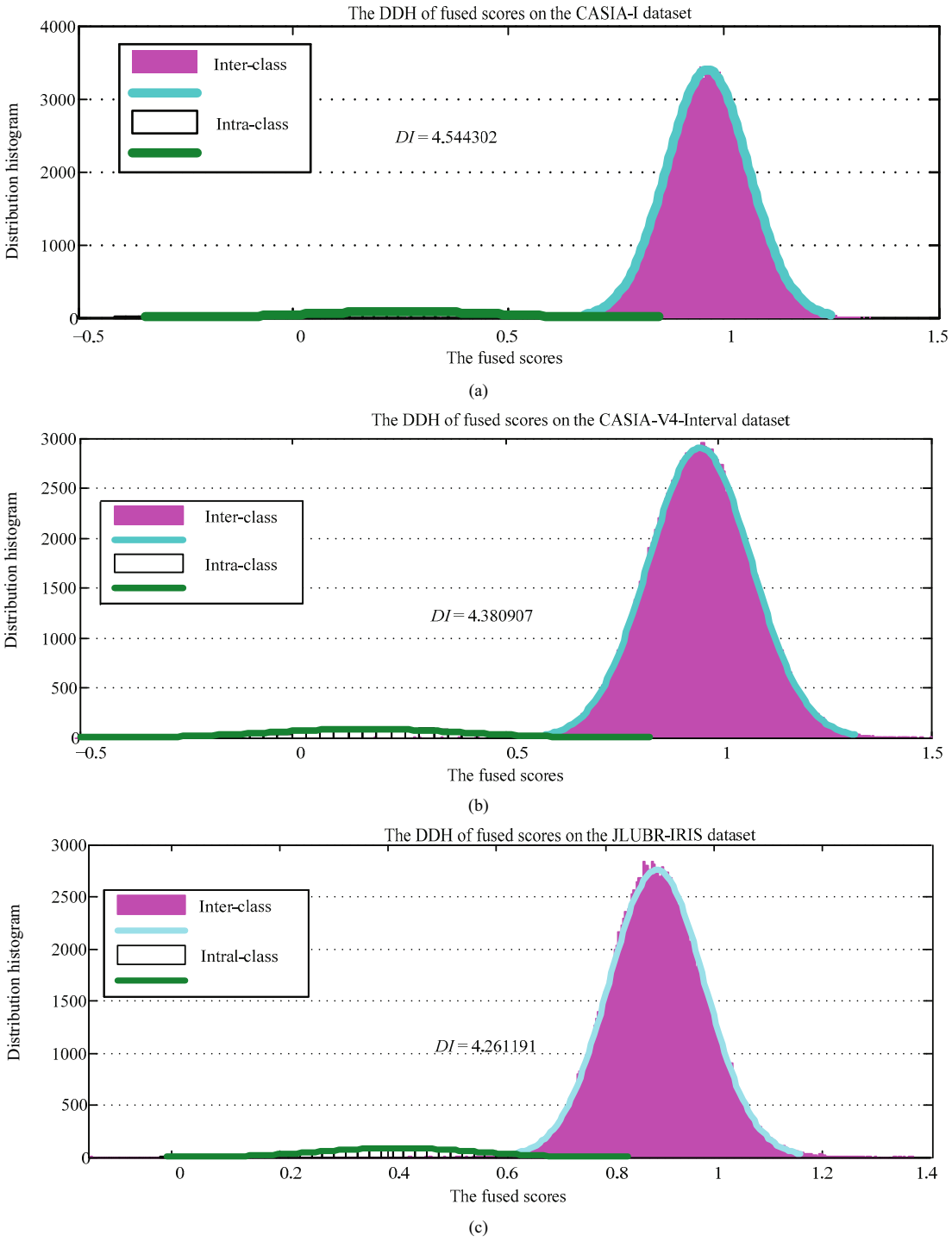

Fig. 12 The DDH of the fused scores on (a) CASIA-I, (b) CASIA-V4-Interval and (c) JLUBR-IRIS.

performance of our proposed methods. In order to achieve unbiased comparative results, the results directly come from several published works. From this table, it is observed that *CCR* 99.51% with *EER* 0.54% of our system reveals a top-class performance with respect to the CASIA-V4-interval dataset. It demonstrates that our system obtain higher discriminative ability than other approaches reported in Table 3. Daugman's system[1] and Ma's system[4] only employed one certain form of Gabor features to represent iris texture, while Ma's system[39] and Roy's system[40] just utilized the geometric detector to search iris geometric properties as iris features. However, they cannot yet compare with our combined bionic Gabor representations. We also list the *CCR* and *EER* from our published literature[7] achieved by the same CASIA-V4-Interval dataset and the same

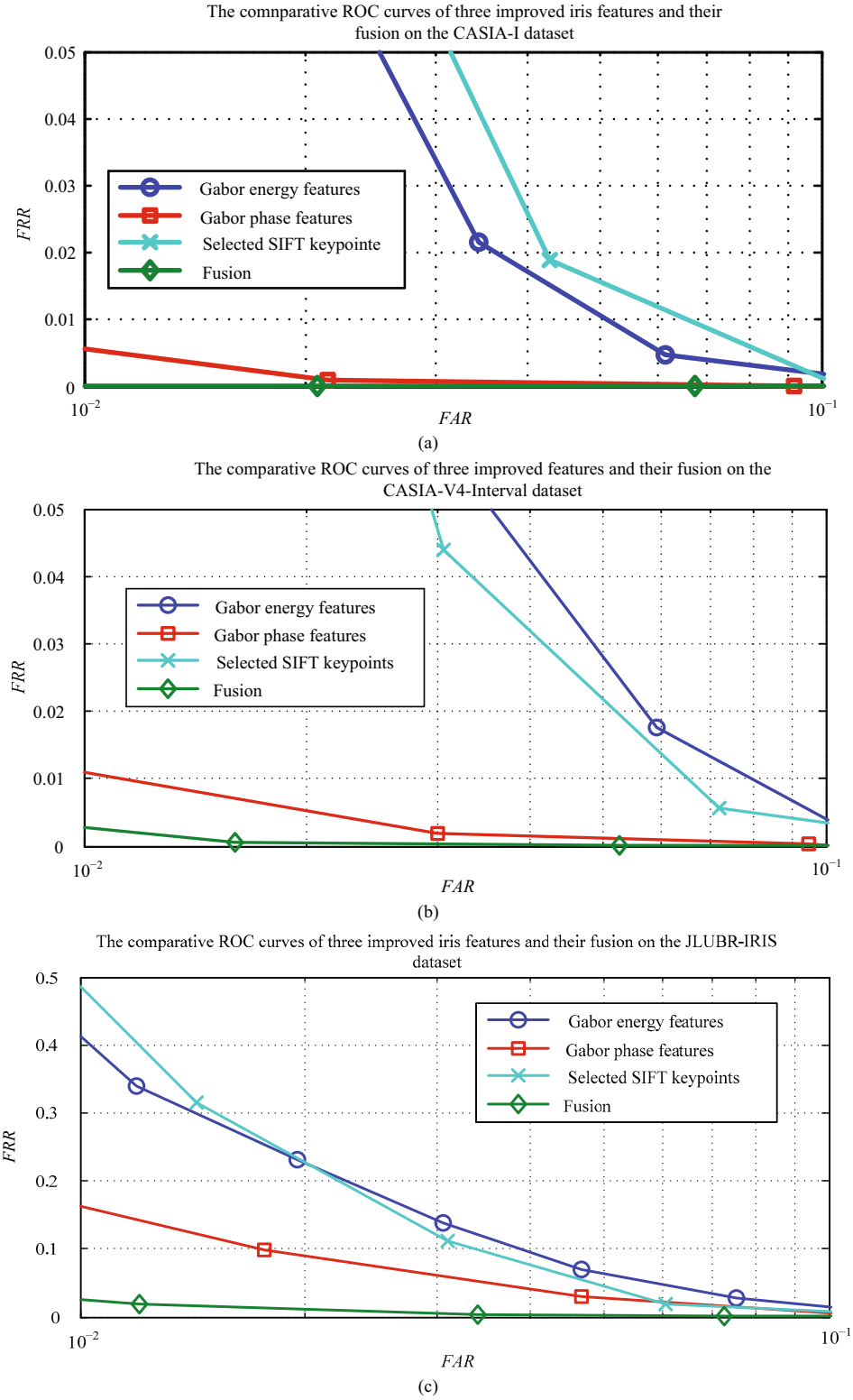

Fig. 13 The comparative ROC curves of fused scores and our proposed single bionic iris features on the (a) CASIA-I, (b) CASIA-V4-Interval and (c) JLUBR-IRIS datasets.

experimental protocols. Because of the limitation to the available training samples on the CASIA-V4-Interval dataset, the outperformance of our previous works is yet to come under the circumstances. Our proposed improved bionic representations, however, may still show their superiority, which benefits from the descriptions of iris texture corresponding to multiple views and their combination strategy.

Table 3 The comparative *CRR*s and *EER*s of our system and some state-of-the-art on the CASIA-V4-interval dataset

Method	*CCR* (%)	*EER* (%)
Daugman[1]	95.19*	1.80*
Ma *et al*.[4]	94.90*	2.62*
Ma *et al*.[39]	95.54*	2.07*
Roy *et al*.[40]	97.21*	0.71*
Liu *et al*.[7]	97.11^	1.03^
Proposed	99.51	0.54

6 Conclusion

In this paper, we improve the characteristics of bionic Gabor representations by combining with SIFT keypoints for iris recognition. Firstly, we select local Gabor energy and phase features, where we investigate a grid searching to find the suitable local block size for the corresponding Gabor responses magnitude and phase, to adequately represent iris texture information. Then we describe the process of SIFT keypoint descriptors and their feature selection strategies. Finally, a SVR-based fusion scheme is designed to project the matching scores of these multiple bionic iris features to a single scalar score for final decision. Three public and self-developed accessible datasets including the CASIA-I, CASIA-V4-Interval and JLUBBR-IRIS datasets are used in a serial of experiments. From the experiments, it can be observed that our improved localized block way may conserve more texture in the process of image division and convolution. Furthermore, our proposed discriminative keypoint selection strategies are able to discard the redundant keypoints and reduce the dimension of corresponding keypoints descriptor representation. The discriminative ability of the two local Gabor features and optimal SIFT keypoints exhibit great improvement, moreover, the multiple bionic feature fusion based on a trained SVR model is able to further achieve encouraging performance compared with the systems using single modal iris features.

Acknowledgments

In this paper, portions of the research use the CASIA-V4-Interval and CASIA-I datasets collected by the Chinese Academy of Sciences' Institute of Automation (CASIA).

References

[1] Daugman J G. High confidence visual recognition of persons by a test of statistical independence. *IEEE Transactions on Pattern Analysis and Machine Intelligence*, 1993, **15**, 1148–1161.

[2] Wildes R P. Iris recognition: An emerging biometric technology. *Proceedings of the IEEE*, 1999, **85**, 1348–1363.

[3] Boles W W, Boashash B. A human identification technique using images of the iris and wavelet transform. *IEEE Transactions on Signal Processing*, 1998, **46**, 1185–1188.

[4] Ma L, Tan T, Wang Y, Zhang D. Personal identification based on iris texture analysis. *IEEE Transactions on Pattern Analysis and Machine Intelligence*, 2003, **25**, 1519–1533.

[5] Proenca H. *Towards Non-Cooperative Biometric Iris Recognition*. PhD Thesis, University of Beira Interior, Portugal, 2006.

[6] Ross A, Jain A K. Multimodal biometrics: An overview. *Proceedings of* 12*th European Signal Processing Conference*, Vienna, Austria, 2004, 1221–1224.

[7] Liu Y, He F, Zhu X, Chen Y, Han Y, Fu Y. Video sequence-based iris recognition inspired by human cognition manner. *Journal of Bionic Engineering*, 2014, **11**, 481–489.

[8] Si Y, Mei J, Gao H. Novel approaches to improve robustness, accuracy and rapidity of iris recognition systems. *IEEE Transactions on Industrial Informatics*, 2012, **8**, 110–117.

[9] Jones J P, Palmer L A. An evaluation of the two-dimensional Gabor filter model of simple receptive fields in cat striate cortex. *Journal of Neurophysiology*, 1987, **58**, 1233–1258.

[10] Proença H, Alexandre L A. Iris recognition: An analysis of the aliasing problem in the iris normalization stage. *IEEE Proceedings of the International Conference on Computational Intelligence and Security*, Guangzhou, China, 2006, **2**, 1771–1774.

[11] Raja Sekar J, Arivazhagan S, Shobana Priyadharshini S, Shunmugapriya S. Iris recognition using combined statistical and co-occurrence multi-resolution features. *International Journal of Pattern Recognition and Artificial Intelligence*, 2013, **27**, 1356001.

[12] Mehrotra H, Majhi B, Gupta P. Robust iris indexing scheme using geometric hashing of SIFT keypoints. *Journal of Network and Computer Applications*, 2010, **33**, 300–313.

[13] Tan T, Zhang X, Sun Z, Zhang H. Noisy iris image matching by using multiple cues. *Pattern Recognition Letters*, 2012, **33**, 970–977.

[14] Gong Y, Zhang D, Shi P, Yan J. Optimal wavelength band clustering for multispectral iris recognition. *Applied Optics*, 2012, **51**, 4275–4284.

[15] Proença H, Santos G. Fusing color and shape descriptors in the recognition of degraded iris images acquired at visible wavelengths. *Computer Vision and Image Understanding*,

2012, **116**, 167–178.

[16] Xu T, Ming X, Yang X. Gabor filter optimization design for iris texture analysis. *Journal of Bionic Engineering*, 2004, **1,** 72–78.

[17] Daugman J. How iris recognition works. *IEEE Transactions on Circuits and Systems for Video Technology*, 2004, **14**, 21–30.

[18] Grigorescu S E, Petkov N, Kruizinga P. Comparison of texture features based on Gabor filters. *IEEE Transactions on Image Processing*, 2002, **11**, 1160–1167.

[19] Wang F, Han J. Information fusion in personal biometric authentication based on the iris pattern. *Measurement Science and Technology*, 2009, **20**, 045501.

[20] Lee J C, Huang P S, Chang J C, Chang C P, Tu T M. Iris recognition using local texture analysis. *Optical Engineering*, 2008, **47**, 067205.

[21] Yu L, Zhang D, Wang K. The relative distance of key point based iris recognition. *Pattern Recognition*, 2007, **40**, 423–430.

[22] Wiskott L, Fellous J M, Kuiger N, Von Der Malsburg C. Face recognition by elastic bunch graph matching. *IEEE Transactions on Pattern Analysis and Machine Intelligence*, 1997, **19**, 775–779.

[23] Kyrki V, Kamarainen J K, Kälviäinen H. Simple Gabor feature space for invariant object recognition. *Pattern Recognition Letters*, 2004, **25**, 311–318.

[24] Bigun J, du Buf J M H. N-folded symmetries by complex moments in Gabor space and their application to unsupervised texture segmentation. *IEEE Transactions on Pattern Analysis and Machine Intelligence*, 1994, **16**, 80–87.

[25] Lee Y L, Kim H C, Park H W. Blocking effect reduction of JPEG images by signal adaptive filtering. *IEEE Transactions on Image Processing*, 1998, **7**, 229–234.

[26] Lowe D G. Distinctive image features from scale-invariant keypoints. *International Journal of Computer Vision*, 2004, **60**, 91–110.

[27] Alonso-Fernandez F, Tome-Gonzalez P, Ruiz-Albacete V, Ortega-Garcia, J. Iris recognition based on sift features. *IEEE Proceedings of the International Conference on Biometrics*, *Identity and Security* (*BIdS*), Tampa, USA, 2009, 1–8.

[28] Kumar A, Passi A. Comparison and combination of iris matchers for reliable personal authentication. *Pattern Recognition*, 2010, **43**, 1016–1026.

[29] Basak D, Pal S, Patranabis D C. Support vector regression. *Neural Information Processing-Letters and Reviews*, 2007, **11**, 203–224.

[30] Schölkopf B, Smola A J. *Learning With Kernels*: *Support Vector Machines*, *Regularization*, *Optimization*, *and Beyond*. MIT Press, Cambridge, MA, USA, 2002.

[31] Vapnik V. The nature of statistical learning theory. *Springer Science & Business Media*, New York, USA, 2000.

[32] JLUBR-IRIS database, [2015-03-12], http://biis.jlu.edu.cn/irisdatabase/.

[33] Specification of cassia iris image database (ver1.0), [2015-03-10] http://www.cbsr.ia.ac.cn/english/IrisDatabase.asp.

[34] Dong W, Sun Z, Tan T. Iris matching based on personalized weight map. *IEEE Transactions on Pattern Analysis and Machine Intelligence*, 2011, **33**, 1744–1757.

[35] Huang Y P, Luo S W, Chen E Y. An efficient iris recognition system. *IEEE Proceedings of the International Conference on Machine Learning and Cybernetics*, 2002, **1**, 450–454.

[36] Ma L, Wang Y, Tan T. Iris recognition based on multichannel Gabor filtering. *Proceedings of the 5th Asian Conference on Computer Vision*, 2002, **1**, 279–283.

[37] Sun Z, Tan T, Qiu X. Graph matching iris image blocks with local binary pattern. *Advances in Biometrics. Springer Berlin Heidelberg*, 2005, 366–372.

[38] Chang C C, Lin C J. LIBSVM: a library for support vector machines. *ACM Transactions on Intelligent Systems and Technology* (*TIST*), 2011, **2**, 27.

[39] Ma L, Tan T, Wang Y, Zhang D. Efficient iris recognition by characterizing key local variations. *IEEE Transactions on Image Processing*, 2004, **13**, 739–750.

[40] Roy K, Bhattacharya P, Suen C Y. Iris recognition using shape-guided approach and game theory. *Pattern Analysis and Applications*, 2011, **14**, 329–348.